Photoexcited Aromatic Reactants Give Multicolor Carbon Nanotube Fluorescence from Quantum Defects

Yu Zheng,[†,§] *Sergei M. Bachilo*,[†] *and R. Bruce Weisman*[*,†,‡]

[†]Department of Chemistry and the Smalley-Curl Institute and [‡]Department of Materials Science and NanoEngineering, Rice University, Houston, Texas 77005, United States

ABSTRACT

Covalent functionalization of single-wall carbon nanotubes (SWCNTs) can be valuable for modifying their electronic and optical properties and creating fluorescent quantum defects. We report here a previously unreported category of such reactions involving interactions of photoexcited aromatic compounds with SWCNT sidewalls. When aqueous suspensions of SWCNTs are exposed to organic aromatic compounds and then irradiated by UV light, fluorescent defects are formed in the nanotubes at rates that depend on the aromatic ring substituents. In reactions with aniline or iodoaniline, strong spectral sidebands appear within one minute. Total SWCNT photoluminescence can be enhanced by a factor as large as ~5. Notably, emission spectra of reacted SWCNTs depend on the presence or absence of dissolved oxygen during the reaction. For (6,5) SWCNTs, treatment when oxygen is present gives an additional emission band red-shifted by 160 meV from the pristine position, whereas treatment without oxygen leads to two

additional emission bands red-shifted by 140 and 270 meV. Variance spectroscopy shows the presence of individual "multicolor" nanotubes with three distinct emission bands (pristine plus two shifted). The facile generation of dual fluorescent quantum defects in SWCNTs provides emission closer to standard telecom wavelengths, advancing the prospects for applications as single-photon sources in quantum information processing.

KEYWORDS

UV photochemistry, single-wall carbon nanotube functionalization, exciton localization, dual shifted photoluminescence, aryl photoreactions

Semiconducting single-wall carbon nanotubes (SWCNTs) are well known for their structure-specific near-IR photoluminescence. There is increasing interest in enhancing the intensity and wavelength versatility of this emission through controlled covalent reactions that create localized quantum defects in the nanotubes. These sites trap mobile excitons and lead to spectrally shifted photoluminescence that holds promise for applications including single-photon emission sources in quantum cryptography.[1-3] Nanotubes with local functionalization have also been shown to display intriguing photophysical properties.[4-8] Reported reactants for preparing such functionalized SWCNTs include ozone or hypochlorite (for oxygen doping),[9,10] diazonium salts,[4,11,12] alkyl or aryl halides,[11,13,14] and guanine nucleobases in SWCNTs coated with single-stranded DNA.[15] The latter method provides spatial and energetic control through selection of the base sequence of the DNA coating.

We report here an additional class of SWCNT functionalization reactions that shift and enhance the nanotube photoluminescence. These covalent reactions proceed in normal aqueous

SWCNT suspensions after the addition of organic aromatic compounds such as nitrobenzene or aniline and irradiation with near-UV light. The photoexcited aromatics react with nearby SWCNTs, converting some sp^2 carbon atoms of the nanotube surface into sp^3-hybridized quantum defects. These reactions proceed efficiently at room temperature under modest UV irradiation intensities. Moreover, we find that the nanotube spectral changes depend dramatically on dissolved oxygen. If purged of dissolved oxygen, treated samples display two distinctly shifted emission features that are assigned to different types of quantum defects. By contrast, reactions in the presence of dissolved oxygen lead to a single shifted emission band.

RESULTS AND DISCUSSION

To introduce sp^3 quantum defects in nanotubes, we prepare an aqueous dispersion of surfactant-suspended SWCNTs and mix with nitrobenzene, iodobenzene, aniline, *p*-iodoaniline, or phenol. These have octanol/water partition coefficients of 71, 1800, 8, 220, and 32, respectively,[16] so they should preferentially partition into the hydrophobic cores of micelles surrounding the nanotubes. The mixtures are then irradiated by light from an LED with fairly broad emission centered near 300 nm, leading to a chemical reaction between the nanotube sidewall and the photoexcited aromatic molecules. Absorption spectra of the reactants show that nitrobenzene, *p*-iodoaniline, and aniline have relatively strong absorption at the irradiation wavelengths while phenol and iodobenzene have weaker but significant absorptions (see Figure S1). We propose that a photoexcited aromatic molecule reacts with an adjacent SWCNT through an electron transfer process to form a covalent bond between its benzene ring and a carbon atom of the nanotube sidewall.

Figure 1 shows the spectrally shifted photoluminescence measured after UV irradiation of a dispersion of CoMoCAT SWCNTs in 1% aqueous sodium dodecylsulfate (SDS) mixed with organic aromatics. As can be seen from Figure 1a, the intensity of the pristine (6,5) peak at 980 nm is greatly reduced while strong shifted bands appear at longer wavelengths. An unexpected finding is the strong oxygen sensitivity of the final spectra. In samples treated while air-saturated, we observe an intense additional emission feature peaking at 1125 nm (denoted E_{11}^{*}). This appears similar to the red-shifted features found in previous studies of oxygen-doped and diazonium-functionalized SWCNTs.[9-11] However, samples treated equivalently after purging with argon to remove other dissolved gases display dual red-shifted emission features peaking at 1105 and 1250 nm (denoted E_{11}^{*} and E_{11}^{**}, respectively). Figure 1 illustrates these spectral transformations for reactions with photoexcited *p*-iodoaniline, nitrobenzene, and aniline.

The altered emission spectra are accompanied by an increase in the Raman D/G band intensity ratio (see Figure S2), as expected when sp^2-hybridized SWCNT carbon atoms are converted to sp^3 hybridization.[17] We also observe that the shifted spectra persist after immersing treated nanotubes in a solution of sodium deoxycholate (SDC), which is known to be a strong surfactant that can displace other noncovalent SWCNT coatings.[18] We infer that the spectrally shifted photoluminescence of treated samples arises from covalent functionalization of SWCNT sidewalls. Compared to samples treated in the presence of dissolved oxygen, those treated after argon purging show slightly smaller E_{11}^{*} red-shifts in addition to the appearance of strong E_{11}^{**} emission. This suggests that different functionalization reactions occur with and without O_2. Our excitation-emission contour plots indicate that treatment causes negligible changes in E_{22} peak wavelengths, consistent with the view that mobile excitons can be formed mainly by absorption in

pristine sections of a nanotube and then emit red-shifted recombination luminescence after becoming trapped at sparse functionalization sites.

We find dual spectrally shifted SWCNT emission bands after oxygen-free photochemical reactions with several aromatic molecules, including *p*-iodoaniline, aniline, nitrobenzene, and phenol (see Figures 1b and S3). By contrast, the reaction between SWCNTs and photoexcited iodobenzene leads only to singly shifted emission under both oxygen-free and air-saturated conditions (see Figures S5 to S8). Iodobenzene differs from the other aromatic reactants because its C-I bond is readily photodissociated to produce the free phenyl radical, which can add to a SWCNT to create sp^3 quantum defects.[13,19] We therefore hypothesize that the dual shifted emission with the other aromatic reactants reflects a mechanism other than radical addition. Further information can be obtained by comparing the functionalization rates with aniline and nitrobenzene. These compounds have similar absorptions at our irradiation wavelength, but the rates of their SWCNT photoreactions differ greatly: optimized conversion is achieved within a few minutes for aniline but requires hours for nitrobenzene. These two aromatics are expected to behave quite differently in electron transfer reactions because aniline's amino group is electron donating while the nitrobenzene's nitro group is electron withdrawing. The large observed difference in reaction rates suggests the role of partial electron transfer from the photoexcited aromatic molecule to the adjacent SWCNT, which would give an excited complex that may lead to covalent bond formation. This proposed mechanism is sketched below as Scheme 1.

Scheme 1

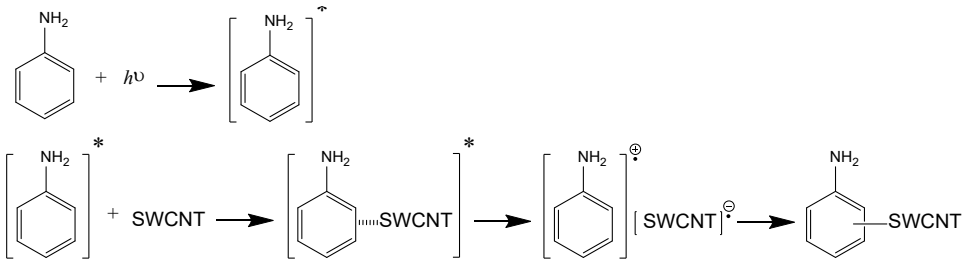

Figure 2 illustrates how the SWCNT spectral changes depend on irradiation time, irradiation power, and reactant concentration for functionalization by nitrobenzene in air-saturated, room temperature samples. Sample emission spectra are plotted as a function of irradiation time in Figure 2a, and it is clear that the intensity of the E_{11}^* emission feature at 1121 nm increases monotonically during 5 h of UV exposure. An unusual effect observed in this system was that the addition of nitrobenzene to SWCNT samples caused a decrease in pristine nanotube emission without UV irradiation. Because this partial quenching was reversed by adding trolox (see Figure S9), a reducing agent,[20] we suspect that it reflects partial p-doping of the nanotube. The partial E_{11} emission quenching was also reversed by UV irradiation prior to significant covalent photofunctionalization. This effect can be seen by comparing the 0 h and 1 h traces in Figure 3c.

We performed control experiments to confirm that the covalent SWCNT functionalization requires UV photoexcitation (see Figures S10 to S12). No spectrally shifted luminescence was observed from SWCNT samples containing nitrobenzene that were stored in the dark or were irradiated at 532 nm, which can excite SWCNTs but not the aromatic reactant. Total nanotube emission, spectrally integrated from 850 to 1500 nm, is plotted as a function of time in Figure 2b for UV-irradiated and for dark control samples (black circles and black triangles, respectively).

The total fluorescence increased by a factor of ~5 after irradiation for ~6 h at a UV power density of approximately 6 mW/cm^2. As shown by the red open squares in Figure 2b, the ratio of E_{11}^* to E_{11} peak intensities increased monotonically from *ca.* 0 to 5.3 after 7 h of irradiation, tracking the strong increase in induced red-shifted emission and concomitant decrease in pristine emission (see Figure S4 for phenol data). The reaction can be accelerated by raising the LED drive current to generate higher UV power. Figure 2c shows that for fixed irradiation time, the spectrally integrated emission and the E_{11}^* / E_{11} intensity ratio both increase monotonically with UV power.

The optimal average concentration of nitrobenzene to induce spectrally shifted luminescence in the SWCNT sample was found to be approximately 0.5 mM (see Figure 2d), although the local nitrobenzene concentration in SWCNT micellar coatings was presumably much higher. Altered emission persists after adding enough SDC to the treated sample to displace other noncovalent coatings on SWCNT surfaces. As can be seen from Figure 2e, fluorescence from the treated sample dispersed in SDC is significantly brighter than from the pristine sample in the same surfactant. We also observed that the photoexcited aromatic treatment generates spectrally shifted emission for SWCNTs dispersed in sodium dodecylbenzene sulfonate (SDBS) or in low concentrations (0.2%) of sodium cholate (SC) (see Figures S13 and S14).

To investigate the source of dual spectrally shifted emission features, we measured fluorescence spectra as a function of irradiation time for argon-saturated SWCNT samples containing aromatic reactants (see Figures 3 and S15). Figure 3a shows that irradiating an oxygen-free sample of CoMoCAT SWCNTs in the presence of *p*-iodoaniline leads to the decrease in pristine E_{11} emission and the growth of dual red-shifted emissions, E_{11}^* and E_{11}^{**}. In Figure 3b we plot the time-dependent kinetics of E_{11}, E_{11}^*, and E_{11}^{**} emission intensities under *ca*. 6 mW/cm^2 of UV irradiation. Pristine E_{11} emission decreases monotonically with irradiation time while the

intensity of E_{11}^{*} emission increases to a maximum at *ca*. 3-5 min before slowly decreasing. The intensity of the second red-shifted emission band, E_{11}^{**}, concurrently increases at a rate slower than the E_{11}^{*} emission and reaches its maximum after *ca*. 10 min of irradiation before decreasing. From the finite initial slopes of the kinetic curves for E_{11}^{*} and E_{11}^{**}, we infer that the two emissive species are formed in parallel processes rather than through sequential conversion of E_{11}^{*} sites into E_{11}^{**} emitters.

In order to highlight emission changes from (6,5) SWCNTs during the reaction, we measured fluorescence spectra using 570 nm excitation in resonance with the (6,5) E_{22} transition. Figures 3c,d show the spectral changes in nanotube emission caused by reaction with photoexcited nitrobenzene molecules in an argon-saturated sample. The (6,5) E_{11}^{*} emission feature peaking at 1102 nm grows with irradiation time and reaches its maximum after *ca*. 1 h of UV irradiation, while the distinct (6,5) E_{11}^{**} emission feature at 1250 nm simultaneously increases at a slower rate and reaches its maximum after *ca.* 2 h of irradiation. As in the *p*-iodoaniline photoreaction, prolonged irradiation decreases the intensities of all three emission features. However, the E_{11}^{*} / E_{11} and E_{11}^{**} / E_{11} intensity ratios increase monotonically with irradiation. As in Figure 3b, the kinetics of E_{11}^{*} and E_{11}^{**} growth suggest that E_{11}^{**} sites are formed directly instead of by conversion of E_{11}^{*} sites.

To assess the coexistence of both types of fluorescent defects in individual nanotubes, we used the recently developed technique of variance spectroscopy, which measures wavelength-dependent fluorescence intensity fluctuations in bulk SWCNT suspensions.[21-23] Correlations between intensity fluctuations at different wavelengths were compiled to construct two-dimensional covariance matrices, which are symmetric about the diagonal. Off-diagonal features in such plots reveal emission from the same particles at two different wavelengths. Figure 4 shows

contour plots of the covariance matrices (measured with a 660 nm diode laser) for CoMoCAT SWCNTs suspended in ~0.5% SDC before treatment and after treatment with photoexcited *p*-iodoaniline in air-saturated and argon-saturated cells. In these samples, the 660 nm excitation leads to emission mainly from (8,3) SWCNTs, giving the dominant peak at 967 nm from the untreated sample (top frame). The absence of off-diagonal features in this covariance plot indicates that few emissive aggregates are present. As shown in the middle frame of Figure 4, the photoreaction under air generates an (8,3) emission feature at 1134 nm and a clear off-diagonal component with coordinates of 967 and 1134 nm, indicating that some individual SWCNTs contribute to both E_{11} and E_{11}*. Quantitative analysis of the covariance data (see Supporting Information) shows that ~98% of SWCNTs in the sample have acquired sp^3 quantum defects, ~81% of which emit only at those defects (E_{11}*) and ~19% of which emit from both pristine regions and defects (E_{11} and E_{11}*). After treatment under argon, samples show dual spectrally shifted luminescence with peaks at 1100 and 1250 nm, visible as strong diagonal features in the covariance plot in the bottom frame. Also present are off-diagonal components with coordinates of 967 and 1100 nm, 967 and 1250 nm, and 1100 and 1250 nm. These indicate that two types of fluorescent defects (E_{11}* giving 1100 nm emission and E_{11}** giving 1250 nm) have formed in individual nanotubes and that excitons can be trapped at either type to give dual spectrally shifted features. Quantitative covariance analysis indicates that essentially none of the SWCNTs in the sample show only pristine emission, ~16.5% of SWCNTs show only E_{11}* emission, ~29% show only E_{11}** emission, ~5% show both pristine and E_{11}* emission, ~0% show both pristine and E_{11}** emission, ~43% show both E_{11}* and E_{11}** emission, and ~7% show emission at all three wavelengths (see Supporting information). These results demonstrate that the photochemical reaction under argon

commonly creates fluorescent defects with different trap depths in individual SWCNTs, giving "multicolor" nanoparticles with unusual spectral heterogeneity.

We find that the E_{11}* fluorescent defects depend on whether the photoreactions occur in the presence or absence of dissolved oxygen. Table 1 summarizes the spectral emission parameters of our pristine and photoreacted (6,5) SWCNTs in SDS suspension. Using the reactants nitrobenzene, aniline, or *p*-iodoaniline, the E_{11}^* peak positions average ~1124 nm for reactions under air but ~1103 nm for reactions under argon, corresponding to a relatively small spectral energy difference of 21 meV. It is known that functionalization of a SWCNT sidewall atom to sp^3 hybridization gives radical character and high reactivity to the 3 neighboring carbon atoms in *ortho* positions and to the 3 in *para* positions.[24] Our calculations confirm that *meta*-functionalization is endoergic, so will not discuss such structures. The *ortho* and *para* positions are illustrated and labeled in Figure 5a. Because the SWCNTs studied here have chiral angles intermediate between zigzag and armchair structures, all 6 of those reaction sites are electronically inequivalent. In agreement with previous quantum computational studies,[3,25,26] our semi-empirical calculations predict that the electronic structure of aryl-functionalized SWCNTs is determined mainly by which of the secondary sites becomes functionalized (*e.g.* with a H atom) rather than by the chemical identity of the second addend. The observed minor oxygen-dependent difference in E_{11}* peak positions may therefore reflect different addend species at the same secondary site. It is not clear why a dependence of E_{11}* wavelength on primary addend substituents, as studied by Wang and co-workers, is seen here for air-saturated but not for argon-saturated samples.

A factor possibly related to the reaction's oxygen sensitivity is that photoexcited nitrobenzene, aniline, and p-iodoaniline all have high quantum yields of triplet state formation.[27] If the triplet state aromatic reacts with the nanotube, for example through cycloaddition,[28,29] both

functionalization sites would become bonded to the aromatic ring. However, in the presence of oxygen, which is an efficient triplet quencher, a different reaction channel might dominate, possibly involving singlet oxygen and leading to peroxide radicals that form carbon-oxygen bonds at one functionalization site. We note that the ~1124 nm (6,5) E_{11}^{*} wavelengths from samples containing dissolved oxygen are similar to wavelengths reported from O-doping and diazonium reactions.[9-11]

The kinetic data shown in Figure 3 indicate that E_{11}^{*} and E_{11}^{**} centers are formed through parallel instead of consecutive reactions. We suggest that those dual red-shifted emission features represent products with different functionalization patterns. We have performed semi-empirical quantum calculations of HOMO and LUMO molecular orbitals and energies for pristine (6,5) nanotubes and for chemically functionalized nanotubes with six aryl-H binding configurations corresponding to placement of the second (H) addend at the six positions relative to the aryl site, as labeled in Figure 5a. The results predict strongly position-dependent HOMO-LUMO gaps, ranging from 205 meV below the pristine value to 171 meV above (see Table S3). We note that some of the most energetically stable structures have predicted HOMO-LUMO gaps greater than the pristine nanotube and would therefore not be able to trap excitons or give red-shifted photoluminescence. It is possible that such structures are present in our reaction products but would not be detectable in emission spectroscopy. Figures 5b,c show computed results for two of the other adducts, with H atoms at positions #5 and #2. Their computed HOMO energies are higher and their LUMO energies are lower as compared to the pristine nanotube. Although we have not performed detailed computations of the corresponding electronic spectra, we assume that smaller HOMO-LUMO gaps correlate with more red-shifted SWCNT photoluminescence. Our results show that the reduction in HOMO-LUMO gap of the functionalized nanotube with the H atom at

position #2 or #4 is nearly twice that of the adduct with H at position #5. This agrees with the findings of Gifford *et al.*[25] (after adjusting structural labels for nanotube orientation) and suggests a correspondence with our observed spectral shifts for the dual emission bands peaking at 1250 nm (E_{11}^{**}, from a structure such as in Figure 5b) and 1102 nm (E_{11}^{*}, from a structure such as in Figure 5c). Although cycloaddition of an aryl reactant would make the second functionalization site a C-C rather than a C-H bond, the spectral shift may be similar because the main factor controlling exciton energy at the defect is apparently the spatial functionalization pattern.[25] Secure identification of the reactive species, product structures, spectral assignments, and reaction mechanisms involved in the photochemical SWCNT functionalization will certainly require additional experiments combined with higher level computational studies.

Table 2 lists spectral characteristics of three different (*n*,*m*) species in an SDS-suspended SWCNT sample before and after reaction with photoexcited nitrobenzene. Although our data span only a narrow range of structures, the spectral red-shifts between E_{11}^{*} and E_{11} show a positive correlation with E_{11}, as was found in the original study of oxygen-doped SWCNTs.[9] The difference in this shift between (6,4) and (6,5) SWCNTs is 75 meV for air-saturated samples compared to 47 meV for the oxygen-free reaction, so it appears that the E_{11}^{*} center formed in the presence of oxygen may be more sensitive to SWCNT structure.

CONCLUSIONS

In summary, we have found a quick and controllable method to create fluorescent quantum defects in SWCNTs by chemical reactions between the nanotube and photoexcited aromatic compounds. Such covalent functionalization leads to spectrally shifted photoluminescence and overall emission enhancement by a factor as large as ~5. The photoreaction is sensitive to the

presence of dissolved oxygen. Air-saturated samples display a single shifted emission band after reaction, but oxygen-free conditions lead to products with two distinct spectrally shifted emission bands arising from different functionalization centers. Variance spectroscopy shows that these centers coexist within individual SWCNTs, giving "multicolor" fluorescent nanoparticles. The dual fluorescent quantum defects generated in oxygen-free photoreactions extend SWCNT defect-state emission to lower photon energies, enhancing their potential for application as single photon sources for quantum information processing at telecommunication wavelengths. Further studies will be needed to uncover the chemical structures and mechanisms involved in the photofunctionalization reactions.

MATERIALS AND METHODS

Sample preparation. Raw CoMoCAT SWCNTs (CHASM Advanced Materials) were added to a solution of 1% (w/v) sodium dodecyl sulfate (SDS) in D_2O. The mixture was kept in a water bath and dispersed using tip sonication at 7 W output power (3 mm tip, Misonix Microson XL) for 30 min active minutes (45 min with duty circle of 40 s on, 20 s off). The suspension was then centrifuged for 90 min at 13000g in a Biofuge-13 (Baxter Scientific). The supernatant was collected and diluted with 1% SDS to the optical density at *ca.* 0.18 for (6,5) E_{11} transition. 1 mM sodium hydroxide (Sigma-Aldrich) was added to the solution to adjust the pH above 7. Aqueous suspensions of SWCNTs dispersed in H_2O solutions containing 0.2% (w/v) sodium dodecylbenzene sulfonate (SDBS) or sodium cholate (SC) were prepared in a similar way. An aqueous solution of 5% (w/v) sodium deoxycholate (SDC) was prepared for use in coating displacement. In this process, centrifugal filtration with a 100 kDa filter removed free dissolved surfactant and the sample was then redispersed into a solution of SDC.

Organic aromatic compounds, including nitrobenzene, aniline, phenol, *p*-iodoaniline, and iodobenzene, were purchased from Sigma-Aldrich. Stock solutions of those organic compounds were dissolved in acetonitrile (Sigma-Aldrich) at a fixed concentration of 50 mM.

Sample functionalization. The aromatic compound stock solutions were added to 500 □L SWCNT suspensions with concentrations of *ca.* 70 μM SWCNT carbon and 0.5 ~ 3 mM aromatic reactant. Air-saturated samples were either treated as is, or were purged with Ar to remove dissolved oxygen. We performed irradiation using a UV LED (Boston Electronics, product code VPC1A1) whose emission ranged from 280 to 340 nm with a peak at 300 nm. The optical power density at the sample was *ca.* 6 mW/cm^2 at a LED drive current of 0.15 A. The drive current was varied to control optical power density at the sample.

Sample characterization. Absorption and short-wave infrared (SWIR) fluorescence spectra were measured in 1 cm path length cells with the prototype model NS2 NanoSpectralyzer (Applied NanoFluorescence, LLC). SWIR fluorescence spectra were excited using diode lasers with fixed excitation wavelengths of 642, 659, and 784 nm.

Two-dimensional excitation-emission contour plots were measured using a custom apparatus. A SuperK EXTREME supercontinuum white light laser source (NKT Photonics) followed by a SuperK Varia (NKT Photonics) filter was used for tunable excitation. This beam was passed through a KG5 filter (Schott) to block stray SWIR emission from the laser. The excitation beam irradiated samples without focusing and with a 10 nm bandwidth, covering wavelengths from 524 to 800 nm with a step size of 2 nm. SWIR emission was collected a 90° angle from excitation directly using a 105 μm core of an optical fiber placed close to the sample. The captured emission was transmitted to a spectrometer (B&WTek Sol 1.7) with a 512-channel

InGaAs array cooled to -15 °C. The instrument and data acquisition were computer-controlled by custom LabVIEW software.

Raman spectra were measured using the prototype model NS3 NanoSpectralyzer (Applied NanoFluorescence, LLC) with a fixed excitation wavelength at 671 nm.

Variance spectra were measured on a step-scan apparatus described in our previous publications.[21-23] Samples were loaded into a cuvette with a 100 μm optical path length. A 660 nm diode laser (Power Technologies, Inc.) followed by a pair of short-pass filters (875 and 1100 nm, Edmund Optics) was used for excitation. 2000 spectra (each integrated for 500 ms) were taken from spatially independent regions of the sample to obtain mean emission and variance spectra. The instrument and data acquisition were computer-controlled by custom LabVIEW software.

Computational methods. Semi-empirical computations were performed on structures optimized using the PM3 method in HyperChem v.7.5 on (6,5) SWCNT model segments with total length slightly less than 4 nm. These segments contained 14 hexagonal rings along the length and included hydrogen atoms passivating dangling bonds at the ends. Changes in relative energies and orbitals between pristine and reacted systems were found very similar to those for 12 ring segments, and not significantly different from longer models.

ASSOCIATED CONTENT

Supporting Information. The Supporting Information is available free of charge on the ACS Publication website. Absorption spectra of the organic compounds; Raman spectra; Fluorescence spectra for SWCNTs treated with phenol and iodobenzene; Excitation-emission contour plots and fluorescence spectra for the treatment of SWCNTs dispersed with SDBS and SC; Kinetics of fluorescence spectra of SWCNTs treated with aniline; Covariance spectra for SWCNTs treated

with nitrobenzene; Variance analysis; Spectral characteristics of SWCNTs treated with *p*-iodoaniline and SWCNTs dispersed in SDC; Computational details.

Financial Interest Statement. The authors declare the following competing financial interest: R.B.W. has a financial interest in Applied NanoFluorescence, LLC, which manufactures some of the instruments in this project.

AUTHOR INFORMATION

Corresponding Author

*E-mail: weisman@rice.edu. Tel: 713-348-3709. Fax: 713-348-5155.

ORCID

Yu Zheng: 0000-0003-2703-9143

Sergei M. Bachilo: 0000-0001-5236-1383

R. Bruce Weisman: 0000-0001-8546-9980

Present Address

§ Yu Zheng: Center for Integrated Nanotechnologies, Materials Physics and Applications Division, Los Alamos National Laboratory, Los Alamos, New Mexico, 87545, USA

ACKNOWLEDGMENTS

This research was supported by grants from the National Science Foundation (CHE-1803066) and the Welch Foundation (C-0807). We are grateful to P. S. Engel for helpful discussions.

REFERENCES

(1) Ma, X.; Hartmann, N. F.; Baldwin, J. K. S.; Doorn, S. K.; Htoon, H. Room-Temperature Single-Photon Generation from Solitary Dopants of Carbon Nanotubes. *Nat. Nanotechnol.* **2015**, *10*, 671-675.

(2) He, X.; Hartmann, N. F.; Ma, X.; Kim, Y.; Ihly, R.; Blackburn, J. L.; Gao, W.; Kono, J.; Yomogida, Y.; Hirano, A.; Tanaka, T.; Kataura, H.; Htoon, H.; Doorn, S. K. Tunable Room-Temperature Single-Photon Emission at Telecom Wavelengths from sp^3 Defects in Carbon Nanotubes. *Nat. Photonics* **2017**, *11*, 577-582.

(3) Saha, A.; Gifford, B. J.; He, X.; Ao, G.; Zheng, M.; Kataura, H.; Htoon, H.; Kilina, S.; Tretiak, S.; Doorn, S. K. Narrow-Band Single-Photon Emission through Selective Aryl Functionalization of Zigzag Carbon Nanotubes. *Nature Chem.* **2018**, *10*, 1089-1095.

(4) Sykes, M. E.; Kim, M.; Wu, X.; Wiederrecht, G. P.; Peng, L.; Wang, Y.; Gosztola, D. J.; Ma, X. Ultrafast Exciton Trapping at sp^3 Quantum Defects in Carbon Nanotubes. *ACS Nano* **2019**, *13*, 13264-13270.

(5) Kwon, H.; Kim, M.; Nutz, M.; Hartmann, N. F.; Perrin, V.; Meany, B.; Hofmann, M. S.; Clark, C. W.; Htoon, H.; Doorn, S. K.; Högele, A.; Wang, Y. Probing Trions at Chemically Tailored Trapping Defects. *ACS Central Science* **2019**, *5*, 1786-1794.

(6) Nutz, M.; Zhang, J.; Kim, M.; Kwon, H.; Wu, X.; Wang, Y.; Högele, A. Photon Correlation Spectroscopy of Luminescent Quantum Defects in Carbon Nanotubes. *Nano Lett.* **2019**, *19*, 7078-7084.

(7) Berger, F. J.; Lüttgens, J.; Nowack, T.; Kutsch, T.; Lindenthal, S.; Kistner, L.; Müller, C. C.; Bongartz, L. M.; Lumsargis, V. A.; Zakharko, Y.; Zaumseil, J. Brightening of Long, Polymer-Wrapped Carbon Nanotubes by sp^3 Functionalization in Organic Solvents. *ACS Nano* **2019**, *13*, 9259-9269.

(8) Brozena, A. H.; Kim, M.; Powell, L. R.; Wang, Y. H. Controlling the Optical Properties of Carbon Nanotubes with Organic Colour-Centre Quantum Defects. *Nature Reviews Chemistry* **2019**, *3*, 375-392.

(9) Ghosh, S.; Bachilo, S. M.; Simonette, R. A.; Beckingham, K. M.; Weisman, R. B. Oxygen Doping Modifies near-Infrared Band Gaps in Fluorescent Single-Walled Carbon Nanotubes. *Science* **2010**, *330*, 1656-1659.

(10) Lin, C.-W.; Bachilo, S. M.; Zheng, Y.; Tsedev, U.; Huang, S.; Weisman, R. B.; Belcher, A. M. Creating Fluorescent Quantum Defects in Carbon Nanotubes Using Hypochlorite and Light. *Nat. Commun.* **2019**, *10*, 2874.

(11) Piao, Y.; Meany, B.; Powell, L. R.; Valley, N.; Kwon, H.; Schatz, G. C.; Wang, Y. Brightening of Carbon Nanotube Photoluminescence through the Incorporation of sp^3 Defects. *Nature Chem.* **2013**, *5*, 840-845.

(12) Shiraki, T.; Shiraishi, T.; Juhász, G.; Nakashima, N. Emergence of New Red-Shifted Carbon Nanotube Photoluminescence Based on Proximal Doped-Site Design. *Sci. Rep.* **2016**, *6*, 28393.

(13) Kwon, H.; Furmanchuk, A.; Kim, M.; Meany, B.; Guo, Y.; Schatz, G. C.; Wang, Y. Molecularly Tunable Fluorescent Quantum Defects. *J. Am. Chem. Soc.* **2016**, *138*, 6878-6885.

(14) Wu, X.; Kim, M.; Qu, H.; Wang, Y. H. Single-Defect Spectroscopy in the Shortwave Infrared. *Nat. Commun.* **2019**, *10*, 2672.

(15) Zheng, Y.; Bachilo, S. M.; Weisman, R. B. Controlled Patterning of Carbon Nanotube Energy Levels by Covalent DNA Functionalization. *ACS Nano* **2019**, *13*, 8222-8228.

(16) Sangster, J. Octanol Water Partition Coefficients of Simple Organic Compounds. *J. Phys. Chem. Ref. Data* **1989**, *18*, 1111-1229.

(17) Graupner, R. Raman Spectroscopy of Covalently Functionalized Single-Wall Carbon Nanotubes. *J. Raman Spectrosc.* **2007**, *38*, 673-683.

(18) Zheng, Y.; Bachilo, S. M.; Weisman, R. B. Enantiomers of Single-Wall Carbon Nanotubes Show Distinct Coating Displacement Kinetics. *J. Phys. Chem. Lett.* **2018**, *9*, 3793-3797.

(19) Wu, X.; Kim, M.; Kwon, H.; Wang, Y. Photochemical Creation of Fluorescent Quantum Defects in Semiconducting Carbon Nanotube Hosts. *Angew. Chem.* **2018**, *130*, 656-661.

(20) Lee, A. J.; Wang, X.; Carlson, L. J.; Smyder, J. A.; Loesch, B.; Tu, X.; Zheng, M.; Krauss, T. D. Bright Fluorescence from Individual Single-Walled Carbon Nanotubes. *Nano Lett.* **2011**, *11*, 1636-1640.

(21) Streit, J. K.; Bachilo, S. M.; Sanchez, S. R.; Lin, C.-W.; Weisman, R. B. Variance Spectroscopy. *J. Phys. Chem. Lett.* **2015**, *6*, 3976-3981.

(22) Sanchez, S. R.; Bachilo, S. M.; Kadria-Vili, Y.; Lin, C.-W.; Weisman, R. B. (*n*,*m*)-Specific Absorption Cross Sections of Single-Walled Carbon Nanotubes Measured by Variance Spectroscopy. *Nano Lett.* **2016**, *16*, 6903-6909.

(23) Zheng, Y.; Sanchez, S. R.; Bachilo, S. M.; Weisman, R. B. Indexing the Quality of Single-Wall Carbon Nanotube Dispersions Using Absorption Spectra. *J. Phys. Chem. C* **2018**, *122*, 4681-4690.

(24) He, X.; Gifford, B. J.; Hartmann, N. F.; Ihly, R.; Ma, X.; Kilina, S. V.; Luo, Y.; Shayan, K.; Strauf, S.; Blackburn, J. L.; Tretiak, S.; Doorn, S. K.; Htoon, H. Low-Temperature Single Carbon Nanotube Spectroscopy of sp^3 Quantum Defects. *ACS Nano* **2017**, *11*, 10785-10796.

(25) Gifford, B. J.; Kilina, S.; Htoon, H.; Doorn, S. K.; Tretiak, S. Exciton Localization and Optical Emission in Aryl-Functionalized Carbon Nanotubes. *J. Phys. Chem. C* **2018**, *122*, 1828-1838.

(26) Gifford, B. J.; He, X.; Kim, M.; Kwon, H.; Saha, A.; Sifain, A. E.; Wang, Y.; Htoon, H.; Kilina, S.; Doorn, S. K.; Tretiak, S. Optical Effects of Divalent Functionalization of Carbon Nanotubes. *Chem. Mater.* **2019**, *31*, 6950-6961.

(27) Freccero, M.; Fagnoni, M.; Albini, A. Homolytic *vs* Heterolytic Paths in the Photochemistry of Haloanilines. *J. Am. Chem. Soc.* **2003**, *125*, 13182-13190.

(28) Hoffmann, N. Photochemical Cycloaddition between Benzene Derivatives and Alkenes. *Synthesis* **2004**, 481-495.

(29) Streit, U.; Bochet, C. G. The Arene-Alkene Photocycloaddition. *Beilstein J. Org. Chem.* **2011**, *7*, 525-542.

Table 1. Emission Features of Photoreacted (6,5) SWCNTs in SDS

Dissolved gas	Aromatic reactant	E_{11} (nm)	E_{11}^{*} (nm)	E_{11}^{**} (nm)	ΔE_{11}^{*} (meV)	ΔE_{11}^{**} (meV)	Reaction time scale
argon	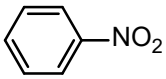	980	1101.5	1250	140	273	hours
	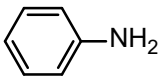	980	1101.5	1250	140	273	minutes
	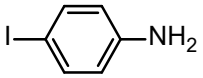	980	1105	1250	143	273	minutes
	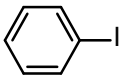	980	1123.5		162		minutes
air	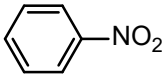	980	1121		159		hours
	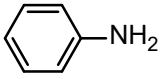	980	1125		163		minutes
	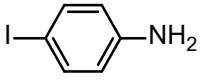	980	1125		163		minutes
	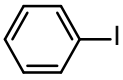	980	1125		163		minutes

Table 2. Comparative Spectral Features of Pristine and Nitrobenezene-reacted SWCNTs

Reaction condition	(*n*,*m*)	E_{11} (nm)	E_{11}^{*} (nm)	E_{11}^{**} (nm)	ΔE_{11}^{*} (meV)	ΔE_{11}^{**} (meV)
argon saturated	(6,4)	878	1012	-	187	-
	(8,3)	956	1086	1250	155	305
	(6,5)	980	1101.5	1250	140	273
air saturated	(6,4)	878	1052		234	
	(8,3)	956	1128		198	
	(6,5)	980	1121		159	

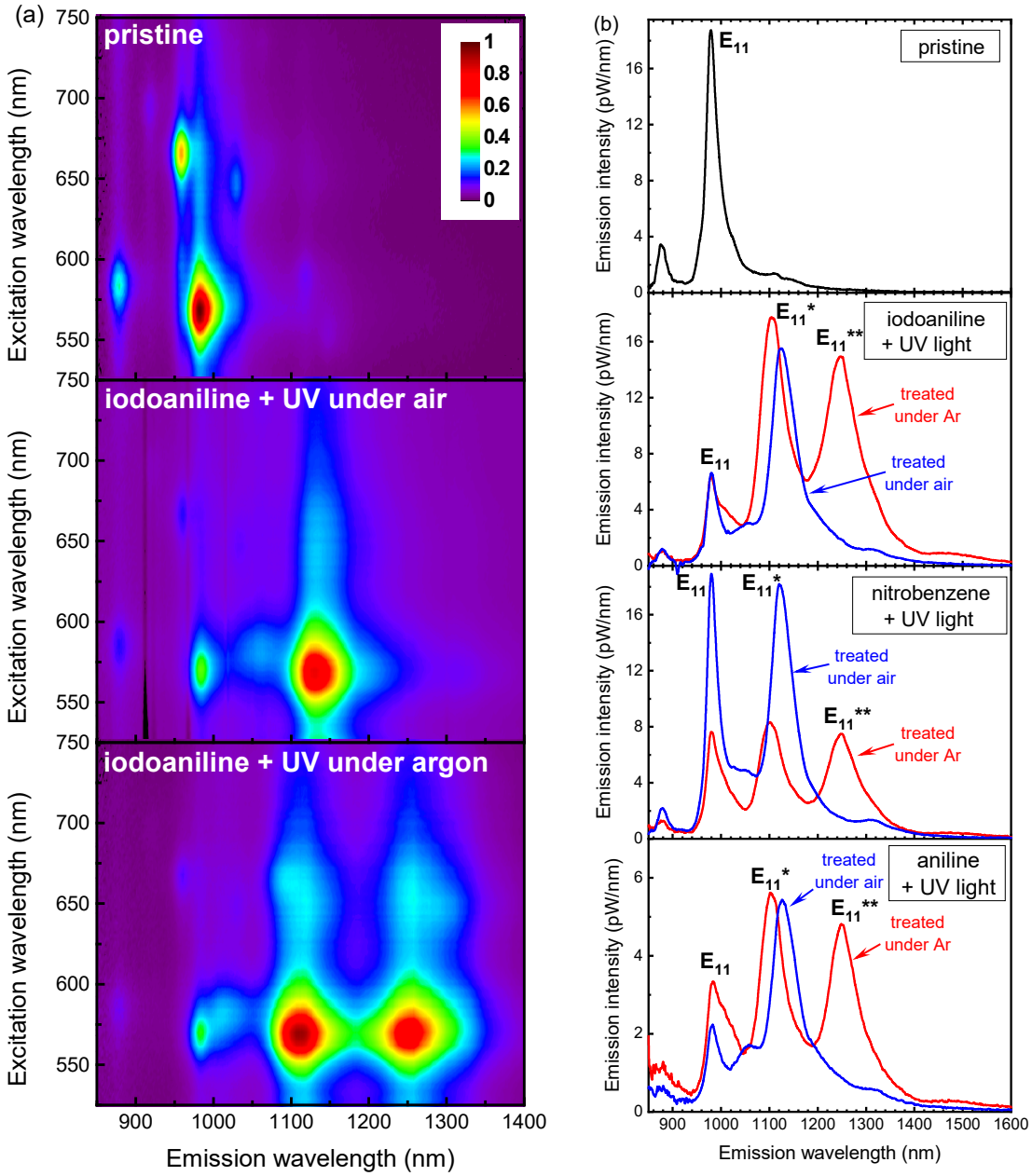

Figure 1. (a) Excitation-emission contour plots for pristine SWCNTs (top frame), the SWCNT sample treated with photoexcited *p*-iodoaniline under air (middle frame), and the sample treated under argon (bottom frame). (b) Emission spectra with 570 nm excitation for (top to bottom): the pristine SWCNT sample; samples treated with photoexcited *p*-iodoaniline; nitrobenzene; and aniline. Blue curves show spectra of air-saturated samples; red curves show spectra of argon-saturated samples.

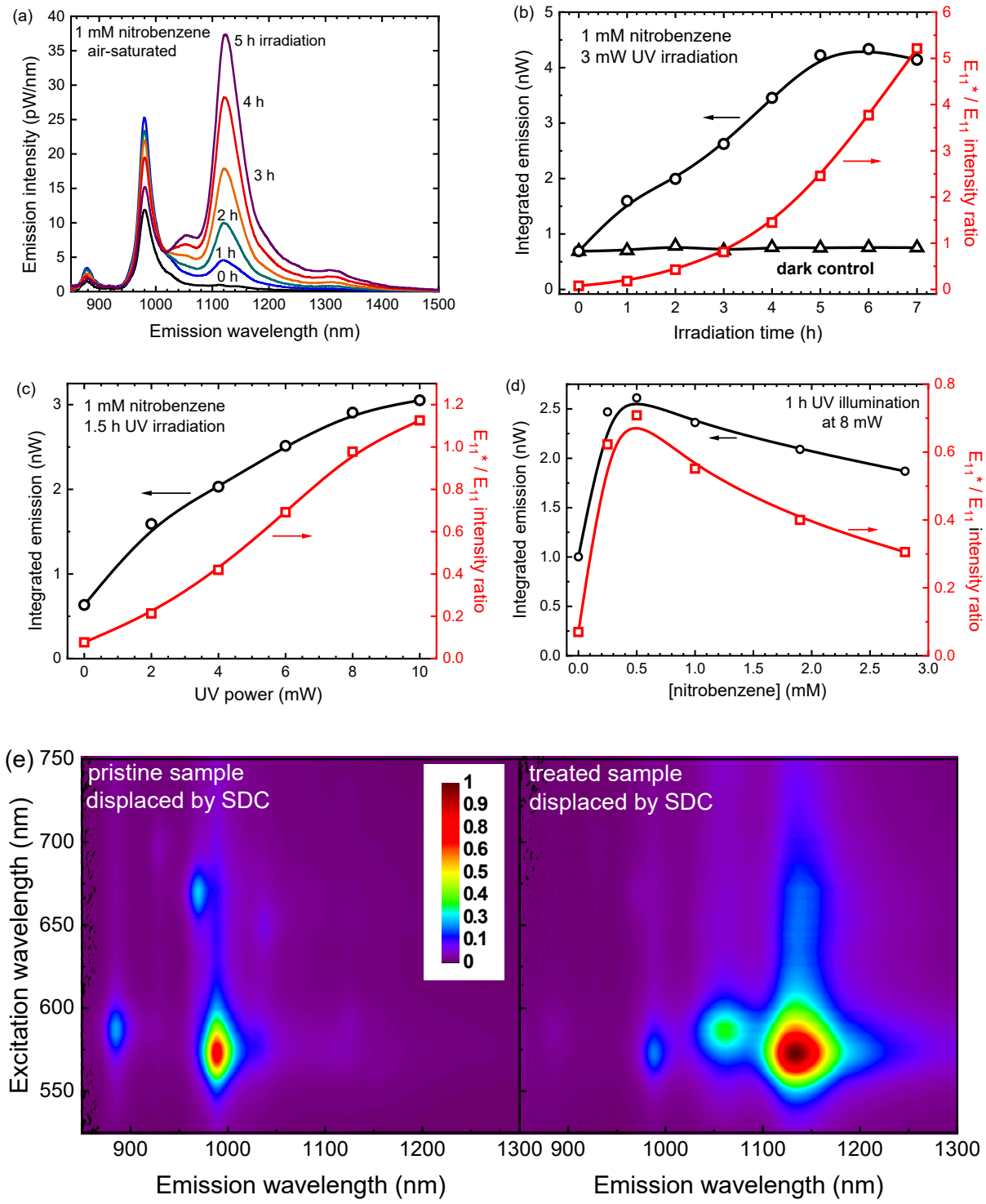

Figure 2. (a) Fluorescence spectra (excited at 570 nm) of an air-saturated sample of SWCNTs containing 1 mM nitrobenzene and irradiated with UV light at room temperature for different times. (b) The spectrally integrated emission (from 850 to 1500 nm) *vs.* UV irradiation time for SWCNT samples containing 1 mM nitrobenzene. Triangles show data for a control sample kept in

dark. Circles show data for the irradiated sample; red squares are the corresponding E_{11}^*/E_{11} emission intensity ratios. (c) Spectrally integrated emission (black circles) and E_{11}^*/E_{11} intensity ratios (red squares) *vs.* approximate UV irradiation power for 1.5 h irradiation and 1 mM nitrobenzene. (d) Spectrally integrated emission (black circles) and E_{11}^*/E_{11} intensity ratios (red squares) *vs*. nitrobenzene concentration for 1 h of 8 mW UV irradiation. (e) Excitation-emission contour plots for the pristine (left) and treated (right) SWCNTs suspended in 0.4% SDC. The intensity color scale applies to both frames.

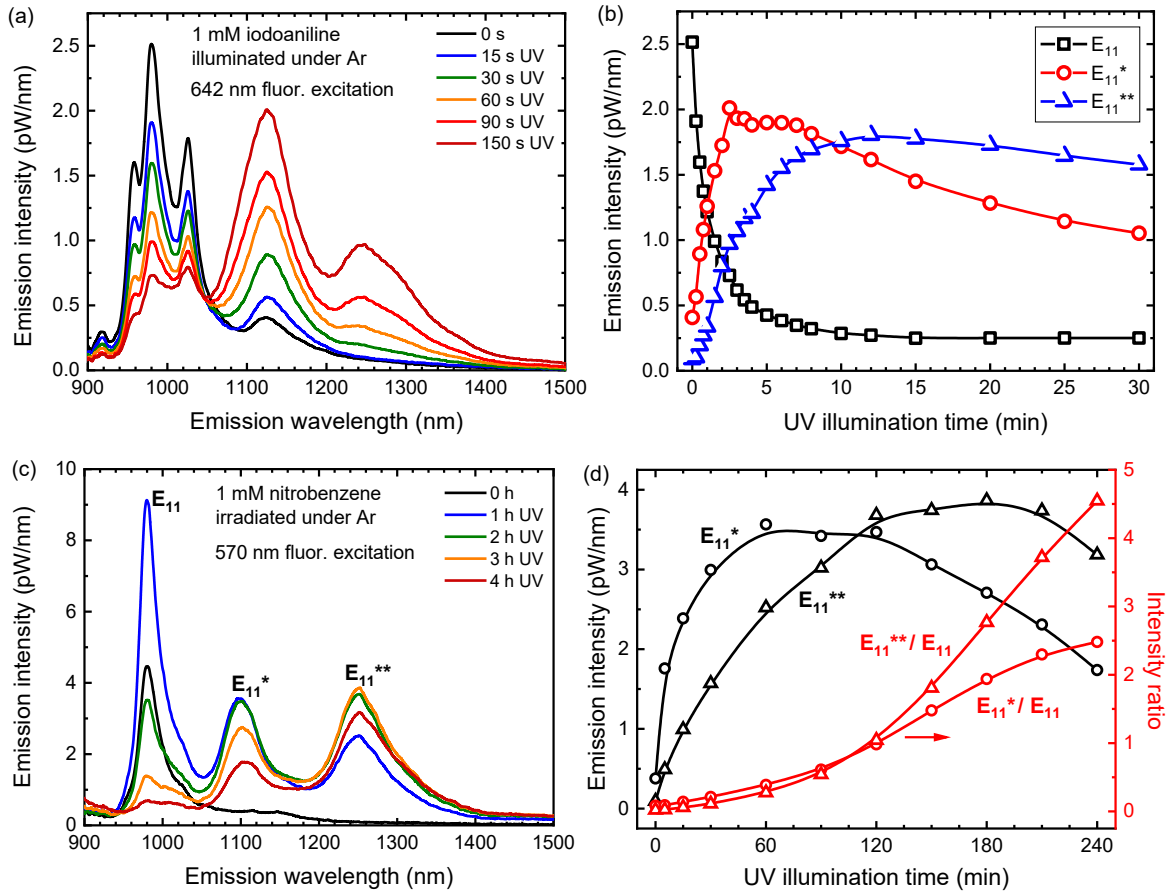

Figure 3. (a) Fluorescence spectra (measured with 642 nm excitation) of an argon-saturated dispersion of CoMoCAT SWCNTs containing 1 mM *p*-iodoaniline that was irradiated with UV light for various times. (b) Intensity kinetics (obtained from (a)) of the pristine E_{11} emission (black curve), the first shifted E_{11}^{*} emission (red curve), and the second shifted E_{11}^{**} emission (blue curve) during irradiation. (c) Fluorescence spectra (measured with 570 nm excitation) of a sample of SWCNTs added with 1 mM nitrobenzene and then irradiated with UV light under argon conditions for different irradiation time. (d) Intensity kinetics (obtained from (c)) of the first shifted E_{11}^{*} emission (open circles), and the second shifted E_{11}^{**} emission (open triangles) during irradiation are shown as black curves. The changes in the emission intensity ratio of E_{11}^{*}/ E_{11} and E_{11}^{**}/ E_{11} with irradiation time are shown as red curves.

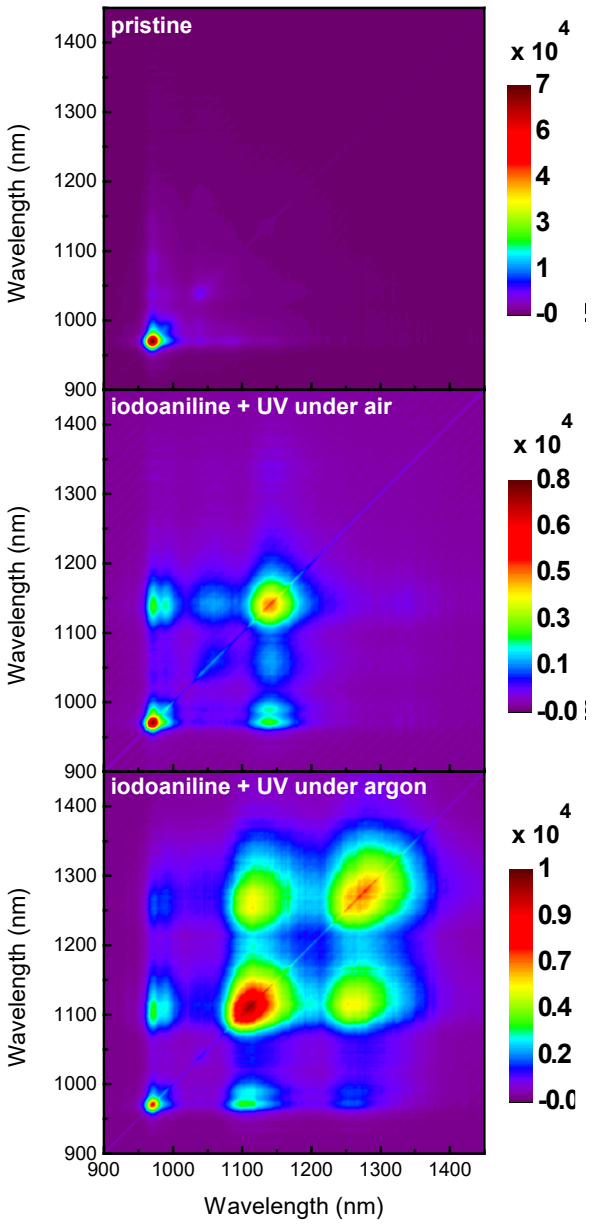

Figure 4. Covariance contour plots (measured with 660 nm excitation) for pristine SWCNTs (top frame), the SWCNT sample treated with photoexcited *p*-iodoaniline under ambient conditions (middle frame), and the sample treated under argon conditions (bottom frame). All of these samples were displaced by 0.4% SDC before the measurements.

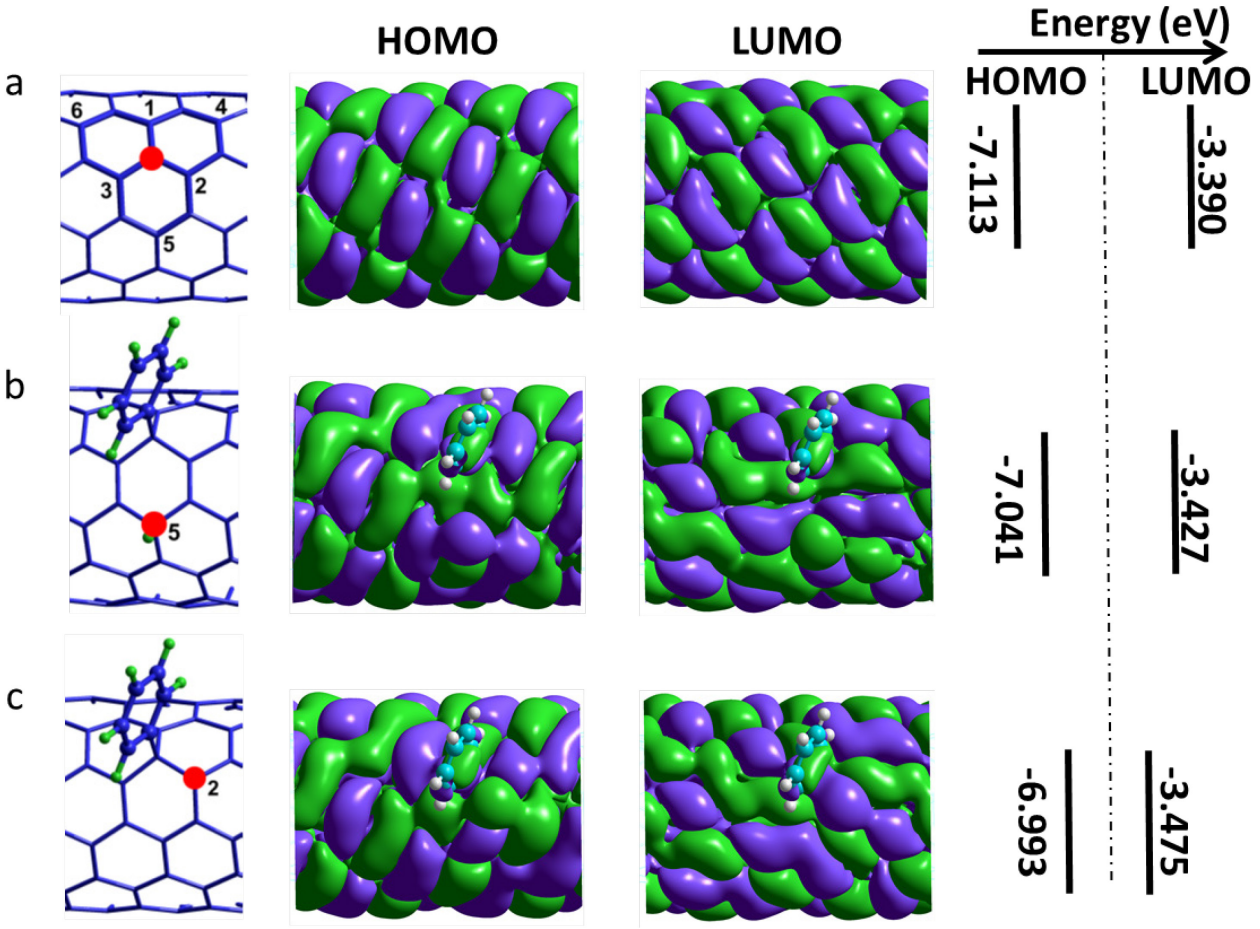

Figure 5. Computed chemical structures, HOMO and LUMO molecular orbitals, and orbital energies of pristine and functionalized (6,5) SWCNTs. In these structures, carbon atoms are shown as blue and hydrogen atoms as green. (a) The pristine nanotube, with a red dot marking the site for primary (aryl) binding and the numbers marking the six possible sites for secondary (hydrogen atom) binding. (b) The covalently functionalized nanotube with a hydrogen atom at position #5 (marked by a red dot). (c) The covalently functionalized nanotube with a hydrogen atom at position #2 (marked by a red dot).

Table of Contents Graphic